frontiers | Frontiers in Physics

REVIEW
published: 11 October 2022
doi: 10.3389/fphy.2022.946515

Fundamentals of Magneto-Optical Spectroscopy

Katsuaki Sato[1]* *and Takayuki Ishibashi*[2]

[1]Faculty of Technology, Tokyo University of Agriculture and Technology, Koganei, Japan, [2]Department of Materials Science and Bioengineering, Nagaoka University of Technology, Nagaoka, Japan

This paper provides a comprehensive review of magneto-optical (MO) spectroscopy. In the first place, different methods of MO measurements such as the Faraday effect, MO Kerr effect, and Cotton-Mouton effect are briefly introduced. Next, macroscopic and microscopic origin in magnetic materials is summarized. In the third part, measuring techniques for MO spectroscopies are reviewed, with a particular reference to the polarization modulation technique.

Keywords: magneto-optics, spectroscopy, electronic structures, measurements, ferromagnet

1 INTRODUCTION

It is well known that light is not influenced by a static magnetic field in a vacuum. On the contrary, light transmitted through materials or reflected by materials is influenced by a magnetic field or by magnetization of materials. These phenomena are called the magneto-optical (MO) effect. In recent years MO effects are utilized for not only optoelectronic devices but also as tools for investigating physical properties and electronic structures of materials. Particularly, MO spectroscopy is important for the latter purposes, since MO effects are originated from optical transitions in the spin-polarized electronic structures of materials.

In the case of transmission geometry, there are two types of magnetic field application, i.e., Faraday configuration in which a magnetic field is applied parallel to the propagation direction of light, and Voigt configuration in which a magnetic field is applied perpendicular to the light propagation.

MO effect in the Faraday configuration is called the Faraday effect, which causes rotation of light polarization (Faraday rotation) and elliptically polarized light (MCD). MO effect in the Voigt configuration is called the Cotton-Mouton effect, which causes magnetically induced birefringence.

MO effect in the reflection geometry is called the magneto-optical Kerr effect (MOKE). In **Figure 1**, three cases of MOKE are illustrated. If the magnetization is normal to the reflection plane, it is called the polar Kerr effect as shown in (a). If the magnetization lies in a plane, two cases exist; i.e., the longitudinal Kerr effect with the magnetization in the plane of light incidence 2) and the transverse Kerr effect with the magnetization perpendicular to the plane of incidence (c).

2 MACROSCOPIC AND MICROSCOPIC ORIGIN OF MAGNETO-OPTICAL EFFECT IN MAGNETIC MATERIALS [1]

2.1 Dielectric Permittivity Tensor of Magnetized Material [2]

Light propagation in a continuous medium can be described in terms of Maxwell's equation, and the response of the medium may be described by the dielectric permittivity (or conductivity, in the case of a metallic medium). We assume relative magnetic permeability μ as unity since the magnetic moment cannot follow the vibration of the frequency of light.

OPEN ACCESS

Edited by:
Rui Min,
Beijing Normal University, China

Reviewed by:
Hang Yin,
Shandong University, China
Hongyi Bai,
Heilongjiang University, China
Wenkai Zhang,
Beijing Normal University, China

***Correspondence:**
Katsuaki Sato
katsuaki.satol@nifty.com

Specialty section:
This article was submitted to Optics and Photonics, a section of the journal Frontiers in Physics

Received: *17 May 2022*
Accepted: *13 June 2022*
Published: *11 October 2022*

Citation:
Sato K and Ishibashi T (2022) Fundamentals of Magneto-Optical Spectroscopy. Front. Phys. 10:946515. doi: 10.3389/fphy.2022.946515

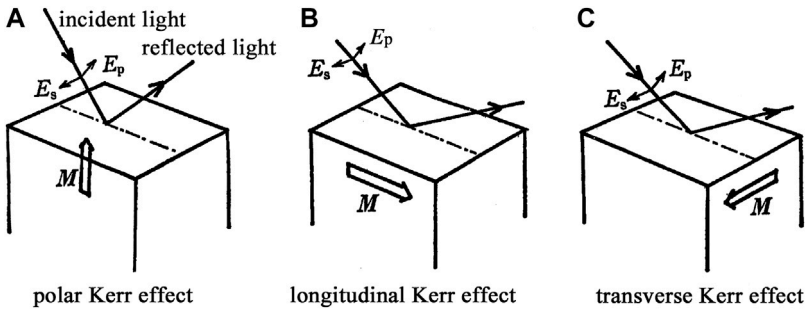

FIGURE 1 | Three types of experimental geometry for MOKE measurement. **(A)** polar Kerr effect, **(B)** longitudinal Kerr effect, and **(C)** transverse Kerr effect.

The dielectric permittivity is a quantity that provides a relation between the electric displacement $\boldsymbol{D}$ and the electric field $\boldsymbol{E}$ as described in **Eq. 1**.

$$\boldsymbol{D} = \varepsilon_0 \hat{\epsilon} \boldsymbol{E} \tag{1}$$

Here ε_0 is the dielectric permittivity of vacuum and $\hat{\epsilon}$ the relative dielectric permittivity tensor as described in **Eq. 2**.

$$\hat{\epsilon} = \begin{bmatrix} \varepsilon_{xx} & \varepsilon_{xy} & \varepsilon_{xz} \\ \varepsilon_{yx} & \varepsilon_{yy} & \varepsilon_{yz} \\ \varepsilon_{zx} & \varepsilon_{zy} & \varepsilon_{zz} \end{bmatrix} \tag{2}$$

Each element of the tensor is a complex as described in **Eq. 3**.

$$\varepsilon_{ij} = \varepsilon_{ij}^{'} + i\varepsilon_{ij}^{''} \tag{3}$$

In the following chapters, we also use an electric conductivity tensor $\hat{\sigma}$ that provides a relation between the electric current density $\boldsymbol{J}$ and the electric field $\boldsymbol{E}$ as described in **Eq. 4**.

$$\boldsymbol{J} = \hat{\sigma} \boldsymbol{E} \tag{4}$$

The electric conductivity tensor can be described as **Eq. 5**.

$$\hat{\sigma} = \begin{bmatrix} \sigma_{xx} & \sigma_{xy} & \sigma_{xz} \\ \sigma_{yx} & \sigma_{yy} & \sigma_{yz} \\ \sigma_{zx} & \sigma_{zy} & \sigma_{zz} \end{bmatrix} \tag{5}$$

Each component of $\hat{\sigma}$ is complex and can be described as **Eq. 6**.

$$\sigma_{ij} = \sigma_{ij}^{'} + i\sigma_{ij}^{''} \tag{6}$$

There holds an equation between the components of $\hat{\sigma}$ and $\hat{\epsilon}$ as **Eq. 7**.

$$\varepsilon_{ij} = \delta_{ij} + i\frac{\sigma_{ij}}{\omega \epsilon_0} \text{ [SI]} \tag{7}$$

If the conductivity is given in CGS unit (s^{-1}) the **Eq. 7** can be rewritten as **Eq. 8**.

$$\varepsilon_{ij} = \delta_{ij} + i\frac{\sigma_{ij}}{\omega} \text{ [CGS]} \tag{8}$$

Here we assume an isotropic medium. Without a magnetic field or without magnetization the dielectric permittivity tensor $\hat{\varepsilon}$ can be expressed as **Eq. 9**.

$$\hat{\epsilon} = \begin{bmatrix} \varepsilon_{xx} & 0 & 0 \\ 0 & \varepsilon_{xx} & 0 \\ 0 & 0 & \varepsilon_{xx} \end{bmatrix} \tag{9}$$

The introduction of a magnetization $\boldsymbol{M}$ along the light propagation direction $\boldsymbol{z}$ causes uniaxial anisotropy to the medium. Then the tensor components of **Eq. 2** can be described as **Eq. 10**.

$$\varepsilon_{xx} = \varepsilon_{yy},\ \varepsilon_{xy} = -\varepsilon_{yx},\ \varepsilon_{xz} = \varepsilon_{yz} = \varepsilon_{zx} = \varepsilon_{zy} = 0 \tag{10}$$

Then the dielectric permeability tensor $\hat{\varepsilon}$ under a uniaxial magnetization, $\boldsymbol{M}$ along z can be expressed by using three tensor elements as **Eq. 11**.

$$\hat{\epsilon}(\boldsymbol{M}) = \begin{bmatrix} \varepsilon_{xx}(\boldsymbol{M}) & \varepsilon_{xy}(\boldsymbol{M}) & 0 \\ -\varepsilon_{xy}(\boldsymbol{M}) & \varepsilon_{xx}(\boldsymbol{M}) & 0 \\ 0 & 0 & \varepsilon_{zz}(\boldsymbol{M}) \end{bmatrix} \tag{11}$$

According to Onsager, the diagonal elements are an even function of $\boldsymbol{M}$ and the off-diagonal elements are an odd function of $\boldsymbol{M}$.

It will be revealed in the following sections that the off-diagonal element $\varepsilon_{xy}(\boldsymbol{M})$ introduces the Faraday effect and MO-Kerr effect while the difference between diagonal elements $\varepsilon_{xx}(\boldsymbol{M})$ and $\varepsilon_{zz}(\boldsymbol{M})$ Cotton-Mouton effect.

2.2 Macroscopic Origin of Magneto-Optical Effect [3, 4]

2.2.1 Faraday Effect

Figure 2 provides schematic illustrations of how Faraday rotation and Faraday ellipticity occur in the medium when a magnetization vector is perpendicular to the plane. In this figure, light propagates vertically to the surface toward the backside, and straight arrows represent electric field vectors of light.

As shown in 1) the electric field vector of the linearly polarized light can be decomposed into two circularly rotating electric field vectors, namely right-circularly polarized light (RCP) and left-circularly polarized light (LCP). If phases of RCP and LCP are different after traveling through a medium of l in length as shown in (b), the trajectory of light composed of two circularly polarized lights becomes a

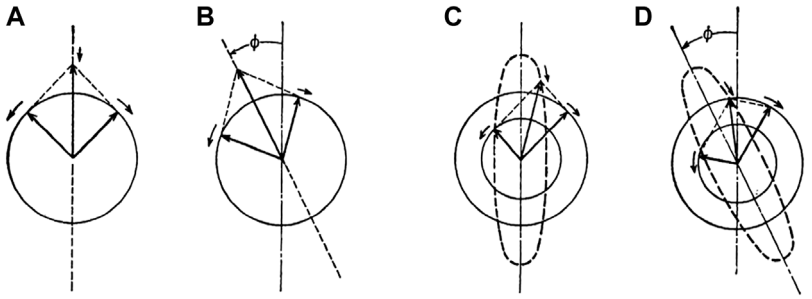

FIGURE 2 | Origin of Faraday rotation and Faraday ellipticity (Magnetic field is applied perpendicular to the surface of the paper **(A)** Linearly polarized (LP) light can be decomposed to right circularly polarized (RCP) and left circularly polarized (LCP) lights **(B)** When the phase of the RCP wave advances faster than that of the LCP wave, composed polarization of the light transmitted three the medium is LP rotated from the incident LP. **(C)** When the amplitude of the RCP wave is larger than that of the LCP wave, composed polarization shows a trajectory of an ellipse. **(D)** When the amplitude and phase of RCP and LCP are different, the trajectory becomes an ellipse with the principal axis inclined.

linearly polarized light which is rotated from the incident light vector. The rotation angle θ_F is given by

$$\theta_F = -(\theta_R - \theta_L)/2 = -\Delta\theta/2 \tag{12}$$

where θ_R and θ_L are phases of RCP and LCP, respectively. On the other hand, if amplitudes of RCP and LCP are different the trajectory of the composed light vector becomes elliptically polarized light, as illustrated in (c). The angle of ellipticity η_F is given by

$$\eta_F = \tan^{-1}\left((E_R - E_L)/(E_R + E_L)\right) \tag{13}$$

where E_R and E_L are amplitudes of RCP and LCP, respectively. In general RCP and LCP suffer differences in both phase and amplitude, which causes an elliptically polarized light with a principal axis rotated from the incident light vector as shown in (d).

The phase difference can be expressed using refractive indices n_+ and n_- for RCP and LCP respectively. Therefore, rotation can be expressed by **Eq. 14**.

$$\theta_F = -\Delta\theta/2 = -\omega l(n_+ - n_-)/c = -\pi\Delta n l/\lambda \tag{14}$$

where $\Delta n = n_+ - n_-$ is the difference between refractive indices for RCP and LCP.

On the other hand, ellipticity or circular dichroism appears if there is a difference between extinction coefficients for RCP and LCP.

$$\eta_F \approx \frac{\exp(-\omega\kappa_+ l/c) - \exp(-\omega\kappa_- l/c)}{\exp(-\omega\kappa_+ l/c) + \exp(-\omega\kappa_- l/c)} \approx -\frac{\pi\Delta\kappa l}{\lambda} \tag{15}$$

where $\Delta\kappa = \kappa_+ - \kappa_-$ is the difference between extinction coefficients for RCP and LCP.

We define complex rotation as $\Phi_F = \theta_F + i\eta_F \approx -\frac{\pi}{\lambda}(\Delta n + i\Delta\kappa)l = -\pi\Delta\hat{N}l/\lambda$,where $\Delta\hat{N}$ is a difference between complex refractive indices for RCP and LCP.

In the following, the Faraday rotation and ellipticity are described in terms of the dielectric permittivity tensor of **Eq. 11**.

Light propagation through the medium with the dielectric permittivity tensor $\hat{\varepsilon}$ can be analyzed using Maxell's equation.

$$\mathrm{rotrot}\boldsymbol{E} = \hat{\varepsilon}\varepsilon_0\frac{\partial^2}{\partial t^2}\boldsymbol{E} \tag{16}$$

We assume that the time- and location-dependence of the electric field and the magnetic field are expressed by the form of $\exp\{-i\omega(t - \hat{N}z/c)\}$. Here the light propagation direction is taken as the z-axis and $\hat{N}$ is the complex refractive constant expressed by $\hat{N} = n + i\kappa$. Then **Eq. 16** can be rewritten as **Eq. 17**.

$$\hat{N}^2\boldsymbol{E} - \hat{\varepsilon}\boldsymbol{E} = 0 \tag{17}$$

The secular equation is

$$\begin{vmatrix} \hat{N}^2 - \varepsilon_{xx} & -\varepsilon_{xy} & 0 \\ \varepsilon_{xy} & \hat{N}^2 - \varepsilon_{xx} & 0 \\ 0 & 0 & -\varepsilon_{zz} \end{vmatrix} = 0 \tag{18}$$

The eigenvalues of the equation are obtained by

$$\left(\hat{N}^2 - \varepsilon_{xx}\right)^2 + \varepsilon_{xy}^2 = 0$$

The solution is

$$\hat{N}_\pm^2 = \varepsilon_{xx} \pm i\varepsilon_{xy} \tag{19}$$

where eigenvalues $\hat{N}_\pm$ are complex refractive indices for RCP (+) and LCP (-), respectively.

The electric field vectors corresponding to $\hat{N}_+$ and $\hat{N}_-$ are RCP and LCP, respectively. Note that if ε_{xy} is zero, optical response is the same for RCP and LCP, meaning that the Faraday effect does not occur.

The difference between complex refractive indices $\Delta\hat{N}$ between RCP and LCP can be expressed as

$$\Delta\hat{N} = \sqrt{\varepsilon_{xx} + i\varepsilon_{xy}} - \sqrt{\varepsilon_{xx} - i\varepsilon_{xy}} \cong i\varepsilon_{xy}/\sqrt{\varepsilon_{xx}} \tag{20}$$

The complex rotation Φ_F can be rewritten as

$$\Phi_F = -\pi\Delta\hat{N}l/\lambda = -i\pi\varepsilon_{xy}l/\sqrt{\varepsilon_{xx}} \tag{21}$$

Then Faraday rotation θ_F and Faraday ellipticity η_F are expressed using refractive index n and extinction coefficient κ as **Eq. 22**.

$$\theta_F = -(\pi l/\lambda)\cdot\left(\kappa\varepsilon_{xy}^{'} - n\varepsilon_{xy}^{''}\right)/\left(n^2+\kappa^2\right)$$
$$\eta_F = -(\pi l/\lambda)\cdot\left(n\varepsilon_{xy}^{'} + \kappa\varepsilon_{xy}^{''}\right)/\left(n^2+\kappa^2\right) \tag{22}$$

Here we used a formula $\varepsilon_{xx} = \hat{N}^2 = (n+i\kappa)^2$.

If we consider a transparent medium, the extinction coefficient κ is zero, then **Eq. 22** becomes very simple as

$\theta_F = -(\pi l/n\lambda)\varepsilon_{xy}^{''}$ and $\eta_F = -(\pi l/n\lambda)\varepsilon_{xy}^{'}$

2.2.2 Polar Kerr Effect

We assume the light beam comes through a vacuum. Using electromagnetic theory, the Fresnel coefficient (complex amplitude reflectance) $\hat{r}_\pm$ for an incident beam of RCP (+) and LCP (-) can be written by **Eq. 23**.

$$\hat{r}_\pm = (\hat{N}_\pm - 1)/(\hat{N}_\pm + 1) \tag{23}$$

We assume $\hat{r}_+ = r_+ exp(-i\theta_+)$ and $\hat{r}_- = r_- exp(-i\theta_-)$ as Fresnel coefficients for RCP and LCP, respectively.

The polar Kerr rotation θ_K and polar Kerr ellipticity are written as

$$\theta_K = -(\theta_+ - \theta_-)/2 = -\Delta\theta/2$$
$$\eta_K = (r_+ - r_-)/(r_+ + r_-) = \Delta r/2r \tag{24}$$

Then complex Kerr rotation $\Phi_K = \theta_K + i\eta_K$ is written using complex Fresnel coefficient as

$$\Phi_K = -\Delta\theta/2 + i\Delta r/2r = -i\Delta\hat{r}/2\hat{r} \tag{25}$$

where $\hat{r} = (r_+ + r_-)/2$ and $\Delta\hat{r} = \hat{r}_+ - \hat{r}_-$.

From **Eq. 25**–**23** we can write complex Kerr rotation by **Eq. 26**

$$\Phi_K = -\varepsilon_{xy}/\left\{(1-\varepsilon_{xx})\sqrt{\varepsilon_{xx}}\right\} \tag{26}$$

This equation suggests that Kerr rotation is enhanced when the denominator takes a small value, i.e., $\varepsilon_{xx} = 1$ or $\varepsilon_{xx} = 0$. This phenomenon occurs in PtMnSb, in which Kerr rotation shows a peak value as large as 2 deg for the photon energy of 1.75eV, where the real part of ε_{xx} crosses zero due to plasma resonance as shown in **Supplementary Figure S1** [5].

This equation provides θ_K and η_K as follows

$$\theta_K = \frac{n\left(1-n^2+3\kappa^2\right)\varepsilon_{xy}^{'} + \kappa\left(1-3n^2+\kappa^2\right)\varepsilon_{xy}^{''}}{\left(n^2+\kappa^2\right)\left\{\left(1-n^2+\kappa^2\right)^2+4n^2\kappa^2\right\}}$$
$$\eta_K = \frac{-\kappa\left(1-3n^2+\kappa^2\right)\varepsilon_{xy}^{'} + n\left(1-n^2+3\kappa^2\right)\varepsilon_{xy}^{''}}{\left(n^2+\kappa^2\right)\left\{\left(1-n^2+\kappa^2\right)^2+4n^2\kappa^2\right\}} \tag{27}$$

2.2.3 Longitudinal Kerr Effect

We assume that the light is incident with an angle of incidence φ_0 to the normal of the medium and proceed in the medium with an angle φ_2. Magnetization is in the plane of the surface and the incident plane. When the p-component is incident, the reflected beam begins to show an s-component in addition to the p-component due to the existence of magnetization. The induced s-component is not in phase with the p-component resulting in elliptically polarized light with the principal axis rotated from the incident beam. A similar effect occurs for incident s-component as well, Complex Kerr rotation Φ_K is given by

$$\tan\Phi_K = r_{sp}/r_{pp} \tag{28}$$

where r_{sp} and r_{pp} are given by

$$r_{sp} = \frac{\varepsilon_{xy}\cos\varphi_0\sin\varphi_2}{\sqrt{\varepsilon_{xx}}\cos\varphi_2\left(\sqrt{\varepsilon_{xx}}\cos\varphi_2+\cos\varphi_0\right)\left(\sqrt{\varepsilon_{xx}}\cos\varphi_0+\cos\varphi_2\right)} \tag{29}$$

$$r_{pp} = \frac{\sqrt{\varepsilon_{xx}}\cos\varphi_0 - \cos\varphi_2}{\sqrt{\varepsilon_{xx}}\cos\varphi_0 + \cos\varphi_2}$$

Snell's law holds between the angle of incidence φ_0 and the angle of refraction φ_2.

$$\sin\varphi_0/\sin\varphi_2 = \sqrt{\varepsilon_{xx}} \tag{30}$$

where φ_0 is real and φ_2 is complex.

2.2.4 Transverse Kerr Effect

When the magnetization vector is vertical to the plane of incidence, the incident s-polarization is subjected to no effect, while incident p-polarization is subjected to a change of reflection intensity. No rotation of polarization occurs for this configuration.

$$r_{pp} = \frac{\varepsilon_{xx}^2\cos\varphi_0 + \left(\varepsilon_{xx}\cos\varphi_2 - \varepsilon_{xy}\sin\varphi_2\right)}{\varepsilon_{xx}^2\cos\varphi_0 + \left(\varepsilon_{xx}\cos\varphi_2 + \varepsilon_{xy}\sin\varphi_2\right)} \tag{31}$$

The reflectivity of intensity is proportional to $|r_{pp}|^2$. Magnetization influences r_{pp} through ε_{xy}.

2.2.5 Cotton-Mouton Effect

The cotton-Mouton effect is a magnetically induced birefringence in the Voigt configuration. Magnetization vector $\boldsymbol{M}$ is perpendicular to the light propagation. The existence of $\boldsymbol{M}$ induces uniaxial anisotropy along the magnetization direction. Assuming the light propagation direction as x, Maxwell's **Eq. 16** leads to the secular **Eq. 32**

$$\left\{\varepsilon_{xx}\left(\varepsilon_{xx} - N^2 + \varepsilon_{xy}^2\right)\right\}\left(\varepsilon_{zz} - N^2\right) = 0 \tag{32}$$

We get two eigenvalues N_1 and N_2 as follows.

$$N_1^2 = \varepsilon_{xx} + \varepsilon_{xy}^2/\varepsilon_{xx}$$
$$N_2^2 = \varepsilon_{xx} \tag{33}$$

Solutions corresponding to N_1 and N_2 are extraordinary waves and ordinary waves, respectively, and give rise to optical retardation $\delta = 2\pi(N_1 - N_2)/\lambda$

2.3 Microscopic Origin of Magneto-Optical Effect

2.3.1 Dielectric Permittivity and Electric Polarization

The electric displacement D in a medium and the electric field E can be related by

$$\boldsymbol{D} = \hat{\varepsilon}\varepsilon_0\boldsymbol{E} = \varepsilon_0\boldsymbol{E} + \boldsymbol{P} \tag{34}$$

where p is the electrical polarization which is related by

$$\boldsymbol{P} = \varepsilon_0\hat{\chi}\boldsymbol{E} \tag{35}$$

Therefore, dielectric permittivity can be expressed in terms of electric polarizability as

$$\hat{\varepsilon} = 1 + \hat{\chi} \tag{36}$$

Electric polarization $\boldsymbol{P}$ is the sum of electric dipole vectors in unit volume. Assuming the density of dipoles as n, the charges as q and -q and displacement by electric field $\boldsymbol{E}$ as $\boldsymbol{u}$, $\boldsymbol{P}$ is expressed as

$$\boldsymbol{P} = nq\boldsymbol{u} \tag{37}$$

2.3.2 Dielectric Permittivity Derived by The Classical Equation of Motion

As explained in **Section 2 2** magneto-optical effect is caused by the off-diagonal element ε_{xy} of the dielectric permittivity tensor $\hat{\varepsilon}$

In the following, we obtain the tensor elements from an equation of motion for a charged particle with mass m and charge q.

$$m\frac{\partial^2\boldsymbol{u}}{\partial t} + m\gamma\frac{\partial\boldsymbol{u}}{\partial t} + m\omega_0^2\boldsymbol{u} = q\left(\boldsymbol{E} + \frac{\partial\boldsymbol{u}}{\partial t}\times\boldsymbol{B}\right) \tag{38}$$

Here γ is a probability of scattering as defined by $\gamma = 1/\tau$, where τ is a scattering lifetime and $m\omega_0^2\boldsymbol{u}$ is a restoring force, where ω_0 is a resonance frequency of the system. The right side represents Lorentz force, where $\boldsymbol{B}$=(0, 0, B) is the magnetic field along z-axis.

Substituting $\boldsymbol{E} = \boldsymbol{E}_0\exp(-i\omega t)$ and $\boldsymbol{u} = \boldsymbol{u}_0\exp(-i\omega t)$ to **Eq. 38** we obtain

$$\begin{aligned} m(\omega^2 + i\omega\gamma - \omega_0^2)x - i\omega qBy &= -qE_x \\ i\omega qBx + m(\omega^2 + i\omega\gamma - \omega_0^2)y &= -qE_y \\ m(\omega^2 + i\omega\gamma - \omega_0^2)z &= -qE_z \end{aligned} \tag{39}$$

where x, y, and z are components of vector $\boldsymbol{u}$ in the Cartesian coordinate.

Substituting solutions of x, y, and z into **Eq. 37** we obtain polarizability tensor elements as

$$\boldsymbol{P} = \varepsilon_0\hat{\chi}\boldsymbol{E} = \varepsilon_0\begin{pmatrix} \chi_{xx} & \chi_{xy} & 0 \\ -\chi_{xy} & \chi_{xx} & 0 \\ 0 & 0 & \chi_{zz} \end{pmatrix}\boldsymbol{E}$$

where tensor elements of $\hat{\chi}$ are given by **Eq. 40**.

$$\begin{aligned} \chi_{xx}(\omega) &= -\frac{nq^2}{m\varepsilon_0}\cdot\frac{\omega^2 + i\omega\gamma - \omega_0^2}{(\omega^2 + i\omega\gamma - \omega_0^2)^2 - \omega^2\omega_c^2} \\ \chi_{xy}(\omega) &= -\frac{nq^2}{m\varepsilon_0}\cdot\frac{i\omega\omega_c}{(\omega^2 + i\omega\gamma - \omega_0^2)^2 - \omega^2\omega_c^2} \\ \chi_{zz}(\omega) &= -\frac{nq^2}{m\varepsilon_0}\cdot\frac{1}{\omega^2 + i\omega\gamma - \omega_0^2} \end{aligned} \tag{40}$$

Here $\omega_c = |q\boldsymbol{B}/m|$ is the cyclotron frequency of charged carrier in the magnetic field $\boldsymbol{B}$.

Using relation 36) the dielectric tensor elements are given by **Eq. 41**.

$$\begin{aligned} \varepsilon_{xx}(\omega) &= 1 - \frac{nq^2}{m\varepsilon_0}\cdot\frac{\omega^2 + i\omega\gamma - \omega_0^2}{(\omega^2 + i\omega\gamma - \omega_0^2)^2 - \omega^2\omega_c^2} \\ \varepsilon_{xy}(\omega) &= -\frac{nq^2}{m\varepsilon_0}\cdot\frac{i\omega\omega_c}{(\omega^2 + i\omega\gamma - \omega_0^2)^2 - \omega^2\omega_c^2} \\ \varepsilon_{zz}(\omega) &= 1 - \frac{nq^2}{m\varepsilon_0}\cdot\frac{1}{\omega^2 + i\omega\gamma - \omega_0^2} \end{aligned} \tag{41}$$

In the following, three cases are discussed (A) $\boldsymbol{B} = 0$, (B) $\boldsymbol{B} = 0$ and $\omega_0 = 0$, (C) $\boldsymbol{B} \neq 0$ and $\omega_0 = 0$.

A) Without magnetic field: Lorentz formula

Eq. 41 becomes simple when $B = 0$ ($\omega_c = 0$) since the off-diagonal term vanishes. If the real and imaginary parts of the permittivity are expressed separately as

$$\begin{aligned} \varepsilon'_{xx}(\omega) &= 1 - \frac{nq^2}{m\varepsilon_0}\cdot\frac{1}{(\omega^2 - \omega_0^2)^2 + \omega^2\gamma^2} \\ \varepsilon''_{xx}(\omega) &= \frac{nq^2}{m\varepsilon_0}\cdot\frac{\omega\gamma}{(\omega^2 - \omega_0^2)^2 + \omega^2\gamma^2} \end{aligned} \tag{42}$$

Figure 3A shows a schematic illustration of spectra for $\varepsilon'_{xx}(\omega)$ and $\varepsilon''_{xx}(\omega)$, the spectral shape of which is dispersion-type and bell-type, respectively.

B) Without magnetic field and without restoring force: Drude formula

If we consider the free carrier motion without magnetic field $\boldsymbol{B}$ and without restoring force, we can assume $\omega_c = 0$ and $\omega_0 = 0$. Then the real and imaginary parts of the permittivity are expressed by

$$\begin{aligned} \varepsilon'_{xx}(\omega) &= 1 - \frac{nq^2}{m\varepsilon_0}\cdot\frac{1}{\omega^2 + \gamma^2} \\ \varepsilon''_{xx}(\omega) &= \frac{nq^2}{m\varepsilon_0}\cdot\frac{\gamma}{\omega^2 + \gamma^2} \end{aligned} \tag{43}$$

Eq. 43 are typical Drude formulas and spectra for $\varepsilon'_{xx}(\omega)$ and $\varepsilon''_{xx}(\omega)$ are shown in **Figure 3B**. The real part of the permittivity takes a large negative value for $\omega \to 0$ and crosses zero at the plasma frequency $\omega'_p = \sqrt{\frac{nq^2}{m\varepsilon_0} - \gamma^2}$ and tends to 1 for $\omega \to \infty$. For $\gamma \to 0$ the free electron plasma frequency is given by $\omega_p = \sqrt{\frac{nq^2}{m\varepsilon_0}}$. In real metals the first term of $\varepsilon'_{xx}(\omega)$ in **Eq. 43** is not unity but should be replaced by ε_∞ introduced by inter-band transitions, then $\omega_p = \sqrt{\frac{nq^2}{m\varepsilon_0\varepsilon_\infty}}$.

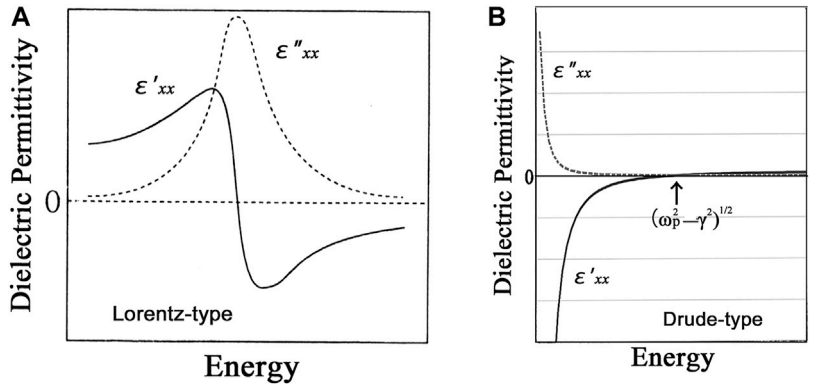

FIGURE 3 | Spectra of dielectric permittivity derived from the classic equation of motion for electrons **(A)** Lorentz-type spectra, **(B)** Drude-type spectra.

C) With non-zero magnetic field and without restoring force: Magneto-plasma resonance and Hall effect

$$\varepsilon_{xx}(\omega) = 1 - \frac{nq^2}{m\varepsilon_0}\cdot\frac{\omega+i\gamma}{\omega\left\{(\omega+i\gamma)^2-\omega_c^2\right\}}$$
$$\varepsilon_{xy}(\omega) = -\frac{nq^2}{m\varepsilon_0}\cdot\frac{i\omega_c}{\omega\left\{(\omega+i\gamma)^2-\omega_c^2\right\}} \tag{44}$$
$$\varepsilon_{zz}(\omega) = 1 - \frac{nq^2}{m\varepsilon_0}\cdot\frac{1}{\omega(\omega+i\gamma)}$$

The second term gives rise to magneto-optical spectra, in which the real part shows a dispersion-type spectrum and the imaginary part a bell-type. If scattering is neglected ($\gamma \to 0$), central frequency exists at the cyclotron frequency ω_c of free carriers.

This case leads to a transport phenomenon of free carriers in the magnetic field. In this case, we should use a conductivity tensor instead of a dielectric permittivity tensor. For this purpose, we use relation $\sigma_{ij} = i\omega\varepsilon_0(\delta_{ij} - \varepsilon_{ij})$. Then we obtain conductivity tensor elements as

$$\sigma_{xx}(\omega) = \frac{nq^2}{m}\cdot\frac{i(\omega+i\gamma)}{(\omega+i\gamma)^2-\omega_c^2}$$
$$\sigma_{xy}(\omega) = -\frac{nq^2}{m}\cdot\frac{\omega_c}{(\omega+i\gamma)^2-\omega_c^2} \tag{45}$$
$$\sigma_{zz}(\omega) = \frac{nq^2}{m}\cdot\frac{i}{\omega+i\gamma}$$

If we assume $\omega = 0$ (DC transport), (**Eq. 45**) lead to the Hall effect

$$\sigma_{xx}(0) = \frac{nq^2}{m}\cdot\frac{\gamma}{\gamma^2+\omega_c^2}$$
$$\sigma_{xy}(0) = \frac{nq^2}{m}\cdot\frac{\omega_c}{\gamma^2+\omega_c^2}$$
$$\sigma_{zz}(0) = \frac{nq^2}{m}\cdot\frac{1}{\gamma}$$

By calculating the inverse matrix, we obtain resistivity tensor elements as

$$\rho_{xx}(0) = \rho_{zz}(0) = m\gamma/nq^2 = 1/\sigma_0$$
$$\rho_{xy}(0) = B/nq == R_H B \tag{46}$$

Here $R_H = 1/nq$ is the Hall coefficient.

2.3.3 Dielectric Permittivity Derived by Quantum Mechanics

In this section, we describe that dielectric permittivity tensor elements are expressed by superposition of dispersion relations based on optical transitions in materials. According to the Kubo formula [6], the electric polarizability tensor element $\chi_{\mu\nu}$ is given by the Fourier transform of the self-correlation function of current density operators. Here the detailed derivation of the equation is omitted here, and only the result is described as follows.

$$\chi_{xx}(\omega) = \lim_{\gamma\to0}\frac{nq^2(\omega+i\gamma)}{\hbar\omega\varepsilon_0}\sum_{n<m}(\rho_n-\rho_m)\frac{2\omega_{mn}|\langle m|x|n\rangle|^2}{\omega_{mn}^2-(\omega+i\gamma)^2}$$
$$= \lim_{\gamma\to0}\frac{nq^2}{m\varepsilon_0}\sum_{n<m}(\rho_n-\rho_m)\frac{(f_{mn})_x}{\omega_{mn}^2-(\omega+i\gamma)^2} \tag{47}$$
$$\chi_{xy}(\omega) = \lim_{\gamma\to0}\frac{-nq^2}{2\hbar\omega\varepsilon_0}\sum_{n<m}(\rho_n-\rho_m)\frac{\omega_{mn}^2\left(|\langle m|x^+|n\rangle|^2-|\langle m|x^-|n\rangle|^2\right)}{\omega_{mn}^2-(\omega+i\gamma)^2}$$
$$= \lim_{\gamma\to0}\left(-\frac{inq^2}{2m\varepsilon_0}\right)\sum_{n<m}(\rho_n-\rho_m)\frac{\omega_{mn}\left(f_{mn}^+-f_{mn}^-\right)}{\omega\left(\omega_{mn}^2-(\omega+i\gamma)^2\right)}$$

Here ρ_n is a probability of occupation of state $|n\rangle$ expressed as

$$\rho_n = \frac{\exp(-\hbar\omega_n/kT)}{\mathrm{Tr}\exp(-H_0/kT)} = \frac{\exp(-\hbar\omega_n/kT)}{\sum_n \exp(-\hbar\omega_n/kT)} \tag{48}$$

and f_{mn} is the oscillator strength of optical transition between the ground state $|n\rangle$ and the excited state $|m\rangle$ and

$$(f_{mn})_x = 2m\omega_{mn}|\langle m|x|n\rangle|^2/\hbar$$
$$(f_{mn})^{\pm} = m\omega_{mn}|\langle m|x^{\pm}|n\rangle|^2/\hbar$$

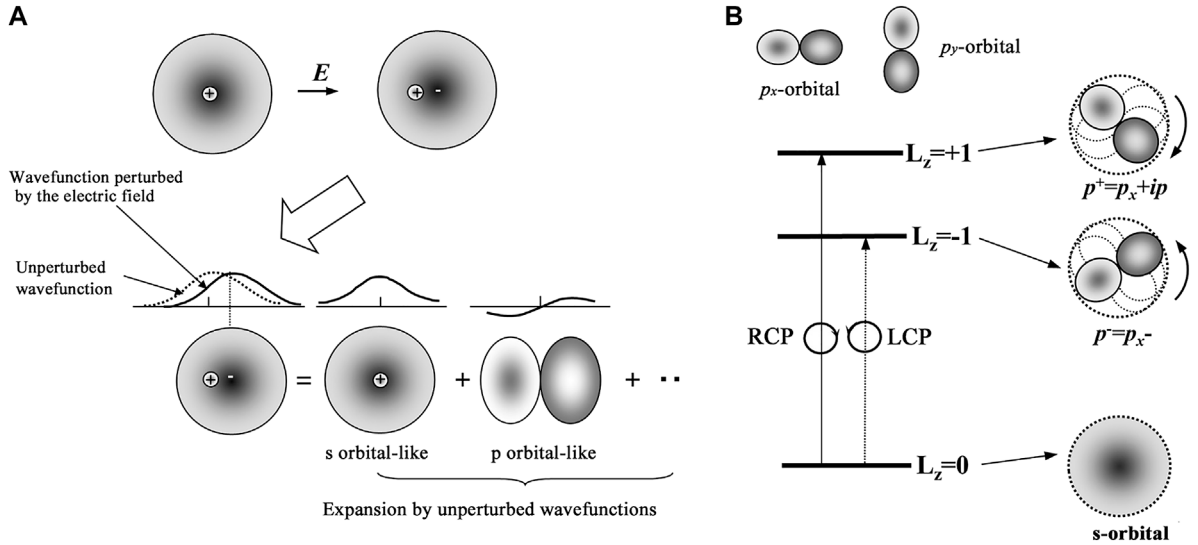

FIGURE 4 | (A) The charge distribution of an atom is altered from an unperturbed state by an application of an electric field as a perturbation, producing an electric dipole moment.**(B)** Schematic illustration explaining the origin of the magneto-optical effect. Angular distribution of electron for Lz = ±1 is considered p-electron-like and can be expressed as $p_\pm = p_x \pm ip_y$ expressing right-hand rotation and left-hand rotations of p-like distribution around the z-axis. This means circularly polarized light induces rotation of electrons.

where qx^+ and qx^- are electric dipole operators for RCP and LCP, respectively.

Electric permittivity can be converted to dielectric permittivity as

$$\varepsilon_{xx}(\omega) = 1 - \frac{nq^2}{m\varepsilon_0}\sum_{n<m}(\rho_n - \rho_m)\frac{(f_{mn})_x}{\omega_{mn}^2 - (\omega + i\gamma)^2} \quad (49)$$

$$\varepsilon_{xy}(\omega) = -i\frac{nq^2}{2m\varepsilon_0}\sum_{n<m}(\rho_n - \rho_m)\frac{\omega_{mn}\Delta f_{mn}}{\omega\left(\omega_{mn}^2 - (\omega + i\gamma)^2\right)}$$

Here $\Delta f_{mn} = f_{mn}^+ - f_{mn}^-$ is a difference in oscillator strengths for RCP and LCP.

At absolute zero temperature $T = 0$, we assume $\rho_n = 1$ and $\rho_m = 0$, then

$$\varepsilon_{xx}(\omega) = 1 - \frac{nq^2}{m\varepsilon_0}\sum_{n<m}\frac{(f_{mn})_x}{\omega_{mn}^2 - (\omega + i\gamma)^2} \quad (50)$$

$$\varepsilon_{xy}(\omega) = -i\frac{nq^2}{2m\varepsilon_0}\sum_{n<m}\frac{\omega_{mn}\Delta f_{mn}}{\omega\left(\omega_{mn}^2 - (\omega + i\gamma)^2\right)}$$

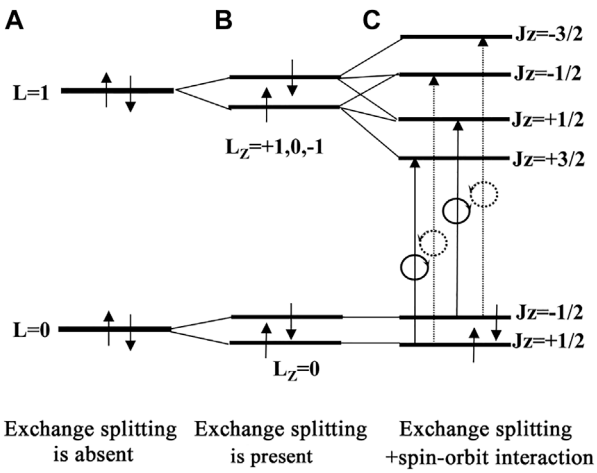

FIGURE 5 | Schematic illustration showing an importance of spin-orbit interaction for magneto-optical effect to occur. **(A)** exchange splitting is absent, **(B)** exchange splitting is present, and **(C)** exchange splitting and spin-orbit interaction are present.

2.3.4 Interpretation of Quantum Mechanical Theory of Dielectric Permittivity

In the following, we make a physical interpretation of why permittivity as shown by (50) can be expressed in terms of optical transitions between electronic states. First, the diagonal element of dielectric permittivity is a quantity showing how easily materials can be polarized by an external electric field. **Figure 4A** illustrates how the charge distribution of an atom is altered from an unperturbed state by an application of an electric field as a perturbation, producing an electric dipole moment. It is well known that any perturbed wavefunctions can be Fourier expanded with unperturbed eigenfunctions. Here coefficients of expansion are given by the oscillator strength and energy nominators $(\omega - \omega_{nm})^{-1}$.

In the second place, we provide physical interpretation for off-diagonal elements of dielectric permittivity. In order to get a non-zero off-diagonal element, Δf_{mn}, or the difference of oscillator strengths for RCP and LCP should exist. In order for electric dipole transition to occur, values of L_z should be different by the unity between the ground and excited states. We assume $L = 0$ for the ground state, then the orbital angular momentum L_z for the

excited state is +1 or -1 as shown in the electronic level diagram of **Figure 4B**. Angular distribution of electrons for $L_z = \pm 1$ is considered p-electron-like and can be expressed as $p_\pm = p_x \pm ip_y$ expressing right-hand rotation and left-hand rotations of p-like distribution around the z-axis. This means circularly polarized light induces rotation of electrons.

In the above discussion, the effect of magnetization has not appeared explicitly. In the following, we treat the effect using the electronic level diagram shown in **Figure 5** Without magnetization energy levels of L_z = +1 and those with L_z = -1 degenerate as shown in **Figure 5A**. Magnetization lifts the spin degeneracy by exchange splitting, giving rise to splitting for the up-spin and down-spin states but does not lift angular orbital degeneracy as in **Figure 5B**. With the spin-orbit interaction, total angular momentum $\boldsymbol{J}$ (=$\boldsymbol{L}$ + $\boldsymbol{S}$) becomes a good quantum number to represent the states as in **Figure 5C**. If the ground state splitting is sufficiently larger than thermal energy kT The ground state is composed of only up-spin electrons, the transition from J_z = +1/2 ground state to J_z = +3/2 occurs by RCP, and the transition from J_z = +1/2 to J_z = -1/2 occurs by LCP. The magneto-optical effect appears if the transition energies of the two transitions are different.

For elevated temperatures transitions from J_z = -1/2 brings about inverse spectral response should be considered considering the distribution of J_z = +1/2 and J_z = -1/2 states.

2.4 Shapes of Magneto-Optical Spectra

2.4.1 Magnetic Insulators[7]

In this subsection, we discuss the shape of magneto-optical spectra in magnetic insulators.

1) Diamagnetic term or two-transition-type spectrum

The energy diagram of **Figure 6A** assumes that the ground state has no orbital degeneracy, and the excited state is split by the spin-orbit interaction. Using **Eq. 50** and assuming $T = 0$, real and imaginary parts of ε_{xy} can be approximated by **Eq. 51**.

$$\varepsilon'_{xy}(\omega) \approx \frac{nq^2\gamma f_0\Delta_{so}}{2m\varepsilon_0\omega}\cdot\frac{\omega_0-\omega}{\left\{(\omega_0-\omega)^2+\gamma^2\right\}^2} \qquad (51)$$
$$\varepsilon''_{xy}(\omega) \approx -\frac{nq^2 f_0\Delta_{so}}{4m\varepsilon_0\omega}\cdot\frac{(\omega_0-\omega)^2-\gamma^2}{\left\{(\omega_0-\omega)^2+\gamma^2\right\}^2}$$

Spectra of ε'_{xy} and ε''_{xy} are illustrated in **Figure 6B**, where the real part shows a dispersion type spectrum, and the imaginary part shows a bell-shaped spectrum with wings on both sides. This type is called "diamagnetic" for historical reasons. Materials with strong magneto-optical effects show spectra of this type in most cases.

2) Paramagnetic term or one-transition-type spectrum

The energy diagram of **Figure 7A** assumes that both ground and excited states are not subjected to splitting in energy, but oscillator strengths $f^\pm$ of transitions between ground and excited states for RCP(+) and LCP(-) are different with a difference Δf. Using **Eq. 50**, real and imaginary parts of ε_{xy} can be approximated by **Eq. 52**.

$$\varepsilon'_{xy}(\omega) \approx \frac{nq^2\gamma\Delta f}{m\varepsilon_0}\cdot\frac{\omega_0}{\left(\omega_0^2-\omega^2+\gamma^2\right)^2+4\omega^2\gamma^2} \qquad (52)$$
$$\varepsilon''_{xy}(\omega) \approx -\frac{nq^2\Delta f}{2m\varepsilon_0}\cdot\frac{\omega_0\left(\omega_0^2-\omega^2+\gamma^2\right)}{\omega\left\{\left(\omega_0^2-\omega^2+\gamma^2\right)^2+4\omega^2\gamma^2\right\}}$$

Spectra of ε'_{xy} and ε''_{xy} are illustrated in **Figure 7B**, where the real part shows a bell-type spectrum and the imaginary part dispersion-type spectrum. This type is called "paramagnetic" for historical reasons. Magneto-optical spectra of spin-forbidden ligand-field transitions mostly show this type.

2.4.2 Magnetic Metals[8]

Optical phenomena in metals should be explained in terms of inter-band transitions. In this case, energy band calculations are employed to obtain eigenvalues and eigenfunctions of band-states in k-space, from which optical responses are calculated using the Kubo formula. For metals, conductivity tensor is used instead of permittivity tensor. We introduce momentum operator

$$\pi = p + \frac{\pi}{4mc^2}\sigma\times\nabla V(r) \qquad (53)$$

Here σ is a spin quantum number, and $\sigma\times\nabla V(r)$ is spin-orbit interaction.

Using $\pi^\pm = \pi^x \pm i\pi^y$, momentum operator for circular polarizations and off-diagonal element of conductivity for infinite scattering lifetime limit are described by **Eq. 54**.

$$\sigma''_{xy}(\omega) = \frac{\pi q^2}{4m^2\hbar\omega}\sum_{l,k}^{occ}\sum_{n,k}^{unocc}\left(|\langle l|\pi^+|n\rangle|^2-|\langle l|\pi^-|n\rangle|^2\right)\delta\left(\omega-\omega_{nl,k}\right) \qquad (54)$$

According to Erskine and Stern, the above formula can be expressed in an integral form on k as **Eq. 55**.

$$\omega\sigma''_{xy} = \frac{\pi q^2}{4m^2\hbar}\cdot\frac{1}{8\pi^3}\int dk^3 F_{nl}(\omega)\delta(\omega-\omega_{nl}) \qquad (55)$$

Here F_{nl} is oscillator strength or transition and can be expressed in terms of optical transition matrix as (56)

$$F_{nl}(\omega) = |\langle n\uparrow|\pi^-|l\uparrow\rangle|^2-|\langle n\uparrow|\pi^+|l\uparrow\rangle|^2+|\langle n\downarrow|\pi^-|l\downarrow\rangle|^2 - |\langle n\downarrow|\pi^+|l\downarrow\rangle|^2 \qquad (56)$$

By defining average transition probability $\bar{F}$ by $\bar{F}_{nl}\int dk^3\delta(\omega-\omega_{nl}) = \int dk^3 F_{nl}(\omega)(\omega-\omega_{nl})$, and introducing joint density of state $J_{nl}(\omega) = \frac{1}{8\pi^3}\int dk^3\delta(\omega-\omega_{nl})$, we get a simple **Eq. 57**.

$$\omega\sigma''_{xy} = \frac{\pi q^2}{4m^2\hbar}\bar{F}_{nl}J_{nl}(\omega) \qquad (57)$$

We define average oscillator strength for RCP and LCR as $\bar{F}^\pm_{nl} = |\langle n\uparrow|\pi^\mp|l\uparrow\rangle|^2-|\langle n\uparrow|\pi^\pm|l\uparrow\rangle|^2$ and joint density of states for RCP and LCP $J^\pm_{nl}$ using $\bar{F}^\pm_{nl}J^\pm_{nl}(\omega) = \frac{1}{8\pi^3}\int dk^3\bar{F}^\pm_{nl}\delta(\omega-\omega_{nl})$ we get

$$\omega\sigma''_{xy} = \frac{\pi q^2}{4m^2\hbar}\left(\bar{F}^-_{nl}J^-_{nl}(\omega)-\bar{F}^+_{nl}J^+_{nl}(\omega)\right) \qquad (58)$$

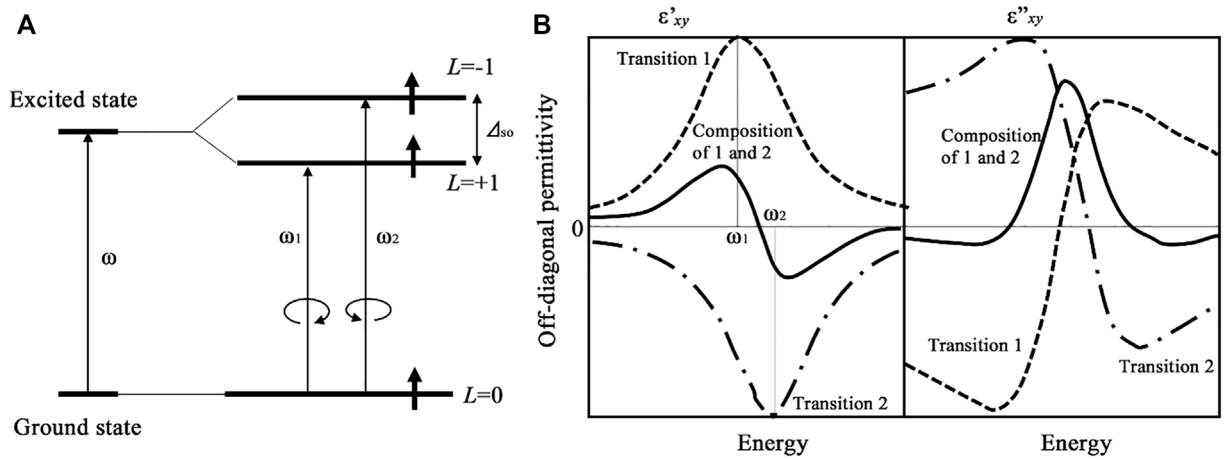

FIGURE 6 | Diamagnetic term of magneto-optical spectra **(A)** Energy level diagram with spin-orbit split excited state **(B)** Diamagnetic spectra of off-diagonal dielectric permittivity elements.

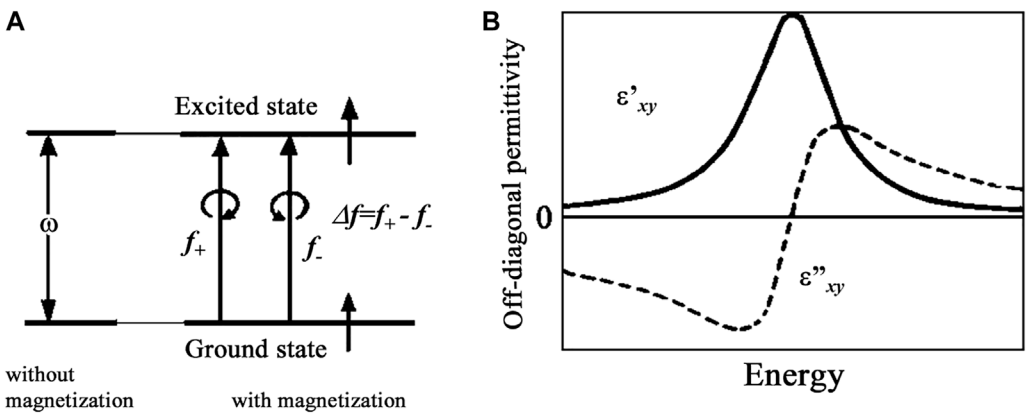

FIGURE 7 | Paramagnetic term of magneto-optical spectra **(A)** Energy level diagram without splitting and with a difference in oscillator strengths for RCP and LCP **(B)** Paramagnetic spectra of off-diagonal dielectric permittivity.

This formula means that the magneto-optical spectrum of metals can be expressed as a difference between inter-band transitions for RCP and LCP.

Figure 8 shows a schematic illustration of the joint density of state (JDOS) spectra for LCP and RCP. Without magnetization JDOSs for LCP and RCP are canceled out as in (a). With a magnetization, the center of gravity of JDOS curves for LCP and RCP shift by ΔE as in (b), resulting in a σ'_{xy} spectrum as shown in (c).

3 MEASUREMENT TECHNIQUES OF MAGNETO-OPTICAL SPECTRA [9]

3.1 Principles of Measurement

3.1.1 Orthogonal Polarizer (Cross Nicol) Technique

The most orthodox technique for evaluation of magneto-optical rotation is the "Orthogonal Polarizer Method", or the so-called "Cross-Nicol Method".

Optical setups are shown in **Figure 9A** for a Faraday configuration in which a magnetic field is applied parallel to the optical path. Let the angle of the optical axis of polarizer P and analyzer A form the vertical axis θ_P and θ_A and Faraday rotation angle of the sample θ_F, then output I of the detector D can be written as **Eq. 59**.

$$I = I_0 \cos^2(\theta_P + \theta_F - \theta_A) \tag{59}$$

For cross nicol condition $\theta_P - \theta_A = \frac{\pi}{2}$, this formula can be rewritten as

$$I = \frac{I_0}{2}(1 - \cos^2\theta_F) \tag{60}$$

When θ_F is proportional to the applied field H, the output I can be plotted against H, from which the Verdet constant can be obtained.

3.1.2 Rotating Polarizer (Analyzer) Technique

This method employs constant rotation of polarizer P or analyzer A. **Figure 9B** shows a case in which the angle of P is fixed, and the

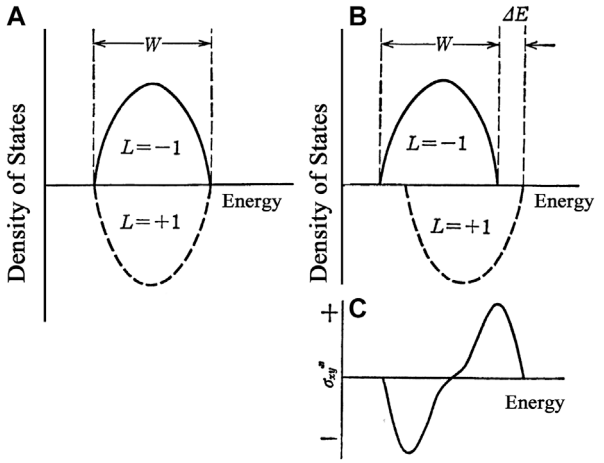

FIGURE 8 | Schematic illustration of band structure and magneto-optical spectra in metals **(A)** Density of state curves of a metal without magnetization **(B)** Density of state curves of a metal with magnetization **(C)** Typical magneto-optical spectrum of a metal with magnetization.

angle of A is rotated with constant angular frequency p. The output I_D of detector D is expressed by **Eq. 61** and doubled frequency signal appears.

$$I_D = I_0 \cos^2(\theta_F - \theta_A) = \frac{I_0}{2}\left(1 + \cos 2\left(\theta_F - pt\right)\right) \tag{61}$$

Faraday rotation angle can be obtained from the phase shift $\Delta\varphi = 2\theta_F$ from zero applied field. Usually, the phase can be measured using a lock-in amplifier.

3.1.3 Oscillating Polarizer (Analyzer) Technique

As shown in **Figure 9C**, the angle of analyzer is oscillated with a small angle amplitude of θ_0 and angular frequency of p

$$\theta_A = \theta_0 \sin pt \tag{62}$$

Then output of D can be expanded using Bessel's function J_n

$$\begin{aligned} I_D &= I_0 \sin^2\left(\theta_0 \sin pt + \theta_F\right) = \frac{I_0}{2}\left\{1 - \cos 2\left(\theta_0 \sin pt + \theta_F\right)\right\} \\ &= \frac{I_0}{2}\left(1 - J_0(2\theta_0)\right)\cos 2\theta_F - I_0 J_1(2\theta_0)\sin 2\theta_F \cdot \sin pt \\ &\quad - I_0 J_2(2\theta_0)\cos 2\theta_F \cdot \cos 2pt \approx \frac{I_0}{2}\left(1 - J_0(2\theta_0)\right) \\ &\quad - 2I_0 J_1(2\theta_0)\theta_F \sin pt - I_0 J_2(2\theta_0)\cos 2pt \end{aligned} \tag{63}$$

Here Faraday rotation is assumed to be small, leading to the last expression. In the above formula, the term with angular frequency p is proportional to the intensity and Faraday rotation and the term with $2p$ is proportional to the intensity, then by taking a ratio of p-component and $2p$-component we can obtain Faraday rotation θ_F.

3.1.4 Faraday Cell Technique

In this method, we use a Faraday cell to compensate Faraday rotation of the sample by using a feedback system. **Figure 9D**

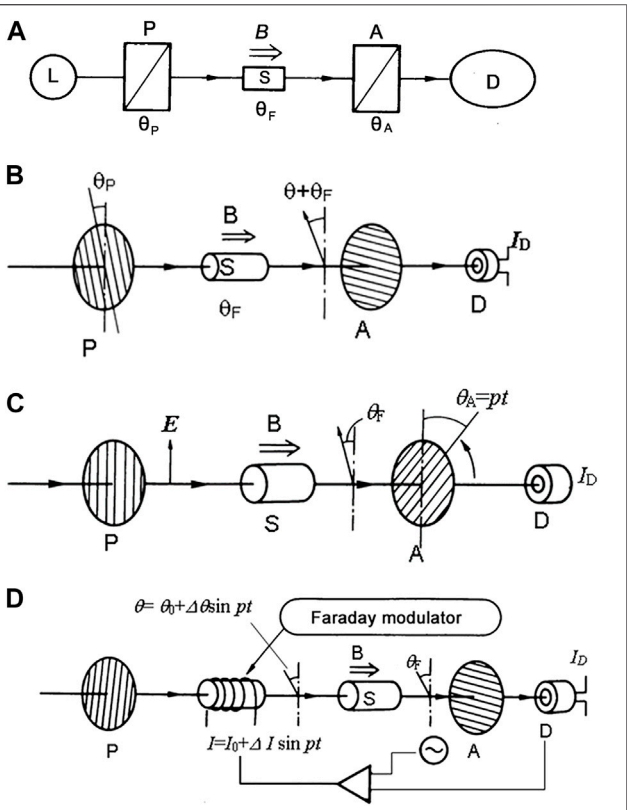

FIGURE 9 | Magneto-optical measurement technique **(A)** Orthogonal polarizer technique L: light source, p: polarizer, S: sample, A: analyzer, D: detector **(B)** Rotating polarizer technique p: rotating polarizer (polarizing angle θ_p, S: sample (Faraday rotation θ_F), A: analyzer, D: detector **(C)** Oscillating polarizer technique p: polarizer, S: sample, A oscillating analyzer, D: detector **(D)** Faraday cell technique p: polarizer, S: sample. A: analyzer, D: detector.

shows an experimental setup, where the optical axis of polarizer P and that of analyzer A are set vertically, leading to zero output in detector D without a sample. The feedback system works to compensate for the Faraday rotation by flowing current to the Faraday cell to keep the output zero. To increase sensitivity, modulating AC current is superposed to the DC current supply for the Faraday cell and the output AC signal detected by a lock-in amplifier is fed to the DC supply. Using the Faraday cell, we can add polarization $\theta = \theta_0 + \Delta\theta \sin pt$ to the system. The output signal I_D for the setup is given by **Eq. 64**.

$$\begin{aligned} I_D &= I_0 \sin^2\left(\theta_0 - \theta_F + \Delta\theta \sin pt\right) \\ &= \frac{I_0}{2}\left\{1 - \cos 2\left(\theta_0 - \theta_F\right)\cos\left(2\Delta\theta \sin pt\right)\right. \\ &\quad \left. + \sin 2\left(\theta_0 - \theta_F\right)\sin\left(2\Delta\theta \sin pt\right)\right\} \approx \frac{I_0}{2}\left(1\right. \\ &\quad \left. - \cos 2\left(\theta_0 - \theta_F\right)J_0(2\Delta\theta)\right) + I_0 \sin 2\left(\theta_0 - \theta_F\right)J_1(2\Delta\theta)\sin pt \\ &\quad - I_0 \cos 2\left(\theta_0 - \theta_F\right)J_2(2\Delta\theta)\cos 2pt \end{aligned} \tag{64}$$

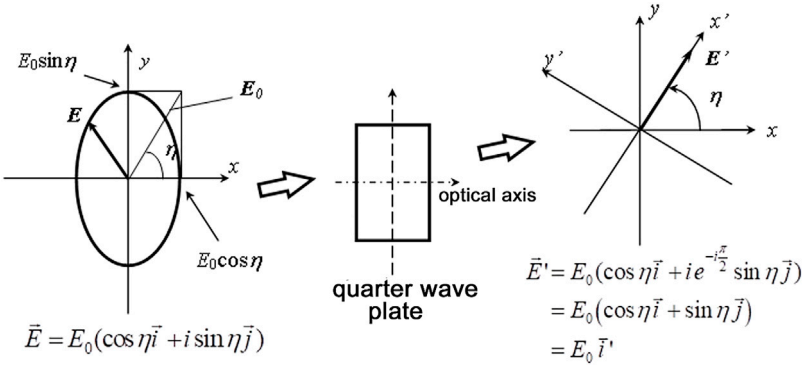

FIGURE 10 | Measurement of ellipticity using a quarter wave plate.

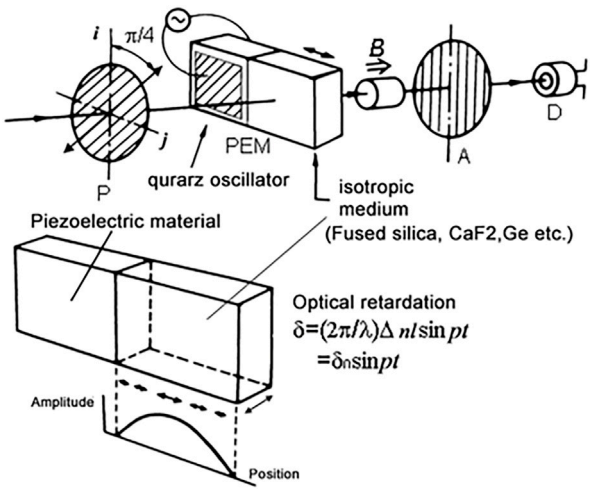

FIGURE 11 | Optical retardation modulation technique.

The p component of the output, which is proportional to $\sin 2(\theta_0 - \theta_F)$, is fed to the DC supply of the Faraday cell to keep the signal zero, i.e., $\theta_0 = \theta_F$. The relation between the DC current and the rotation is calibrated in advance. This method is a so-called "Null method" and provides a precise value of rotation. Although this method is superior to those in the previous sub-sections, there are drawbacks such as the influence of the magnetic field of the Faraday cell, the effect of temperature increase to compensate for a large rotation, and the small Verdet constant in the long wavelengths.

3.1.5 Measurement of Ellipticity

Magneto-optical ellipticity or magnetic circular dichroism (MCD) can be measured using magneto-optical measurement techniques introduced in sub-sections 3.1.1–3.2.4 by introducing a quarter wave plate in front of the analyzer.

As shown in **Figure 10**, we assume that light with an ellipticity η is incident to a quarter wave plate, then incident elliptically polarized electric vector can be expressed as $\boldsymbol{E} = E_0(\cos\eta\boldsymbol{i} + i\sin\eta\boldsymbol{j})$, where $\boldsymbol{i}$ and $\boldsymbol{j}$ are unit vectors with x and y diction. We assume light propagates along the z-axis. When the light passes through a quarter wave plate with an optical axis along x, the light emitted through the wave plate can be expressed as (65).

$$E' = E_0(\cos\eta\boldsymbol{i} + i\exp(-i\pi/2)\sin\eta\boldsymbol{j}) = E_0(\cos\eta\boldsymbol{i} + \sin\eta\boldsymbol{j}) \quad (65)$$

The emitted light is a linearly polarized light rotated by angle η from the x-axis as shown in the left figure.

In this way, we can convert an elliptically polarized light to a linearly polarized light with an inclination of ellipticity. However, for spectroscopic measurement for a wide wavelength region, the quarter wave plate should be changed for different wavelengths. Use of a Babinet-Soleil compensator is recommended.

3.1.6 Optical Retardation Modulation Technique—Simultaneous Measurement for Both Rotation and Ellipticity [10, 11]

For spectroscopic measurement of both rotation and ellipticity, we recommend the use of the optical retardation modulation technique, as illustrated in **Figure 11**.

We use a piezo birefringent modulator (commercially sold PEM = photo-elastic modulator) to modulate optical retardation. The polarization axis of polarizer P should be set to be 45° inclined to the optical axis of the PEM, while that of analyzer A parallel to the optical axis of the PEM. Assuming modulated optical retardation as $\delta = \delta_0 \sin pt$, the output of detector D can be expressed as (66).

$$\begin{aligned} I_D &= \frac{I_0}{2}\{1 - 2\eta_F \sin(\delta_0 \sin pt) - \sin 2\theta_F \cos(\delta_0 \sin pt)\} \\ &\approx \frac{I_0}{2}\{1 - 2\theta_F J_0(\delta_0)\} + I_0 \cdot 2\eta_F J_1(\delta_0)\sin pt - I_0 \\ &\quad \cdot 2\theta_F J_2(\delta_0)\cos 2pt \end{aligned} \quad (66)$$

By taking the ratio of the p-component and DC component, we obtain ellipticity, and the ratio of the $2p$-component and DC component gives rotation. Therefore, we can obtain both ellipticity and rotation simultaneously.

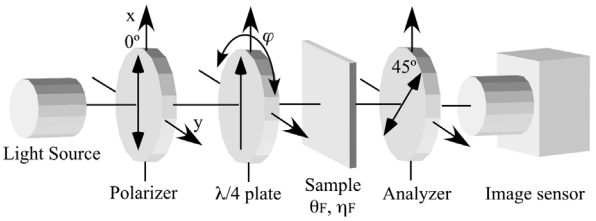

FIGURE 12 | Schematic drawings of MO microscopes using a quarter wave plate and an LCM.

Assuming modulation amplitude of optical birefringence of PEM as Δn, optical retardation described as $\delta_0 = 2\pi\Delta nl/\lambda$ may be subjected to wavelength dependence. We can control the optical birefringence of PEM by an externally applied electric voltage to suppress the wavelength-dependence between 0.2 and 2 μm.

To calibrate the rotation angle, we remove the sample, and the polarization angle of *p* is adjusted to be nearly vertical where the minimum output of the 2*p*-component is obtained. Then the analyzing angle is rotated from +2° to -2° by a step of 1.0° and the value of the ratio of 2*p*-component and DC component is recorded. By taking the difference between the values for the analyzer angles of the same absolute values with different signs (e.g., +1° and -1°), the calibrated value per unit angle is obtained.

For calibration of ellipticity, a retardation plate made of sapphire is employed. A sapphire crystal plate of 0.295 mm thickness was cut along the crystal plane which assures double refraction. If we set the optic axis of the sapphire plate in the vertical direction and the polarizing direction of the analyzer at ± 45° the spectral dependence of the ratio of *p*-component to DC-component shows an oscillating spectral dependence, maxima, and minima appearing at wavelengths where retardation becomes $\pi/2$, the envelope providing a calibration function.

3.1.7 Magneto-Optical Imaging Using Liquid Crystal Modulator [12]

In the case of MO imaging, lock-in detection cannot be employed since image sensors such as the CCD camera cannot respond to the modulation frequency of the PEM. Instead of the lock-in detection, the difference between two images corresponding to different polarization states is calculated by using an image-processing technique, which is equivalent to the PEM-lock-in method described in the previous sub-section. To generate different polarization states, we use a liquid crystal modulator (LCM). Schematic drawings of MO microscopes using a λ/4 plate and an LCM are shown in **Figure 12**.

In the following, we explain a principle of the polarization-modulation MO imaging technique in terms of the Jones matrix method. Each optical component shown in **Figure 12** is expressed in terms of a Jones matrix.

A matrix of the polarizer with its optic axis parallel to the vertical axis 10) is expressed by

$$\boldsymbol{P} = \begin{pmatrix} 1 & 0 \\ 0 & 0 \end{pmatrix}$$

Jones matrix for the LCM in which retardation δ can be controled by an applied voltage can given by

$$\boldsymbol{J}_L = \frac{1}{2}\begin{pmatrix} e^{i\delta/2} + e^{-i\delta/2} & e^{i\delta/2} - e^{-i\delta/2} \\ e^{i\delta/2} - e^{-i\delta/2} & e^{i\delta/2} + e^{-i\delta/2} \end{pmatrix} = \begin{pmatrix} \cos\delta/2 & i\sin\delta/2 \\ i\sin\delta/2 & \cos\delta/2 \end{pmatrix}$$

where LP, RCP and LCP correspond to δ = 0, π/2 and -π/2, respectively.

For a Faraday configuration shown in **Figure 12**, a matrix of a sample having Faraday rotation θ_F and Faraday ellipticity η_F is expressed by

$$\boldsymbol{S} = \begin{pmatrix} \cos\theta_F + i\eta_F \sin\theta_F & -\sin\theta_F + i\eta_F \cos\theta_F \\ \sin\theta_F - i\eta_F \cos\theta_F & \cos\theta_F + i\eta_F \sin\theta_F \end{pmatrix}$$

An analyzer with an optical axis of 45° is

$$\boldsymbol{A} = \frac{1}{2}\begin{pmatrix} 1 & 1 \\ 1 & 1 \end{pmatrix}$$

Using these matrices, an output signal $\boldsymbol{E}_2$ using the LCM can be calculated by

$$\boldsymbol{E}_2 = \boldsymbol{ASJ}_L\boldsymbol{PE}_1$$

Consequently, an intensity measured at a detector is a square of the absolute value of $\boldsymbol{E}_2$ as a function of θ_F, η_F and δ, as **Eq. 67**.

$$I(\theta_F, \eta_F, \delta) = \left(\left|e^{i\delta}\cos\theta_F + \sin\theta_F\right|^2 + \eta_F^2\left|e^{i\delta}\sin\theta_F - \cos\theta_F\right|^2\right)\frac{|E_x|^2}{2} \quad (67)$$

Images of Faraday rotation θ_F and ellipticity η_F can be reconstructed from three images for different polarization states, LP, RCP and LCP, by calculating at each pixel using the following formulae.

$$\theta_F = \frac{1}{2}\sin^{-1}\left\{\frac{2I_{LP} - (I_{LCP} + I_{RCP})}{(1-\eta_F^2)|E_x|^2}\right\} \quad (68)$$
$$\eta_F = \frac{1}{2}(I_{LCP} - I_{RCP})\Big/|E_x|^2.$$

where I_{LP}, $I_{RCP,}$ and I_{LCP} are intensities at each pixel for LP, RCP, and LCP, respectively. For small values of θ_F and η_F less than a few degrees, **Eq. 68** can be reduced to simple expressions (69) by replacing $|\mathbf{E}_x|^2$ with (I_{LCP} + I_{RCP}) as follows,

$$\theta_F \approx (1/2)\{2I_{LP} - (I_{RCP} + I_{LCP})\}\Big/\left\{\left(1-\eta_F^2\right)(I_{RCP} + I_{LCP})\right\} \quad (69)$$
$$\eta_F \approx (1/2)(I_{LCP} - I_{RCP})\Big/(I_{LCP} + I_{RCP})$$

Optical retardation can be modulated in a few tenths of a second by changing AC voltages applied to the LCM, which provides a possibility of real-time imaging using the polarization modulation technique.

3.2 Spectroscopic Measurements

3.2.1 Spectroscopic Measurement of Polar MOKE by Optical Retardation Modulation Technique

Figure 13 provides a measurement setup for the polar magneto-optical Kerr effect for a wide spectral region from near-ultraviolet

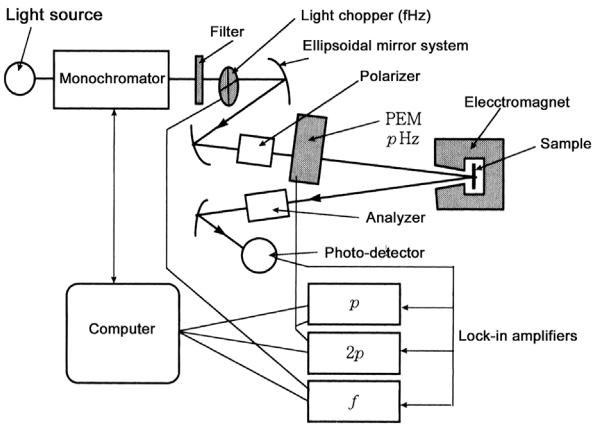

FIGURE 13 | Spectroscopic measurement setup for polar magneto-optical Kerr effect for wide spectral region from near-ultraviolet to near infrared region.

to near-infrared region. The system consists of a light source, a monochromator, a polarizer, a photo-elastic modulator, an analyzer, ellipsoidal mirrors, and a detector. As the light source, we use a halogen tungsten lamp for the visible to infrared wavelength region and a Xenon lamp for the near-ultra-violet ~ visible ~ near-infrared region. The halogen tungsten lamp shows a flat spectral distribution, while the Xenon lamp has a high light intensity for the short wavelength region but has a drawback of line spectra in the near-infrared region. For wavelengths shorter than 200 nm a deuterium lamp is employed. For the monochromator, we select one with a small f-number (f = 3–4) At the expense of high resolution. It is common to prepare two or three diffraction gratings with different blaze-wavelengths according to the wavelength region. Since xenon lamps bring stray light to the monochromator, it is desirable to use a double-monochromator. For the spectroscopic measurement in a wide wavelength region, it is desirable to construct the light condensing system using ellipsoidal mirrors with less chromatic aberration. As a polarizer and analyzer, we recommend the use of a MgF_2-made Rochon prism polarizer. Since this type of polarizer has a double image, a slit is used to cut unnecessary polarization. Finally, as a detector, we use a photomultiplier with a compound-semiconductor cathode having lowered affinity for 200–1800 nm. For longer wavelengths, we use a cooled CdHgTe photodiode.

3.2.2 Spectroscopic Measurement Using A Multi-Channel Spectrometer [13]

Figure 14 shows a schematic diagram of the MO spectrometer utilizing the polarization modulation method with a multichannel spectrometer. A halogen lamp is used as a light source, and a multi-channel spectrometer having a detection range of 350–1000 nm, with a 2048-element linear silicon CCD array detector, is used as a light detector.

For the MO measurement, collimating lenses (L1, L2, L3), pinhole (ph), polarizer (P), perforated electromagnet (EM), and an analyzer (A) were used. A quarter wave plate (Q) was used to carry out the polarization modulation method. The Q will be rotated by a stepping motor. The transmission axis of the analyzer (α) forms an angle of 45° with the polarizer, and the Q will be set to −45°, 0°, and +45° with the polarizer for the measurement.

The procedure of measurement of the Faraday rotation and Faraday ellipticity spectra is as follows. While applying a magnetic field to the sample, the optical axis of the Q is set to −45°, 0°, and +45°, corresponding to left-circularly, linearly and right-circularly polarized light, respectively. Those three polarized light intensity spectra were measured, and Faraday rotation angle (θ_F) and Faraday ellipticity angle (η_F) are calculated by the following **Eq. 69**,

$$\theta_F \approx \frac{1}{2}\left\{\frac{2I_0 - (I_{45} + I_{-45})}{I_{45} + I_{-45}}\right\} \qquad (70)$$

$$\eta_F = -\frac{1}{2}\left\{\frac{I_{45} - I_{-45}}{I_{45} + I_{-45}}\right\}$$

where $I_{-45°}$, $I_{0,}$ and $I_{45°}$ are light intensities when the optical axis of the Q is −45°, 0°, and 45°. The units of the values obtained by **Eq. 70** are radians.

3.2.3 Analysis to Obtain the Off-Diagonal Element of Permittivity Spectrum From Experimental Data

As described in **section 2**, MO effects are derived from the off-diagonal element ε_{xy} as well as the diagonal element ε_{xx} of electric permittivity tensor. Real and imaginary parts of permittivity are obtained from spectra of optical constants (n and κ) measured by a spectroscopic ellipsometer. However, commercial spectroscopic ellipsometer covers wavelength-range from 300 to 800 nm, Spectra of optical constants for a wider spectral region can be obtained from the spectrum of reflectivity R measured at synchrotron facilities using a numerical analysis as shown as follows.

In the analysis, we calculate the spectrum of phase shift $\Delta\theta$ subjected at reflection by using the Kramers–Kronig formula as shown in **Eq. 71**.

$$\Delta\theta(\omega) = \frac{\omega}{\pi}\wp\int_0^\infty \frac{\ln R(\omega')}{\omega'^2 - \omega^2}d\omega' \qquad (71)$$

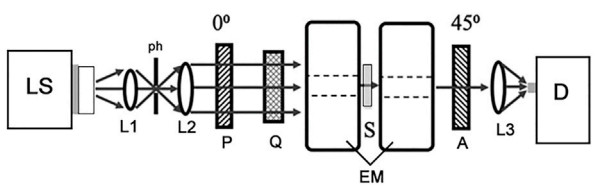

FIGURE 14 | Schematic diagram of the MO spectrometer utilizing the polarization modulation method with a multichannel spectrometer. LS: light source (halogen tungsten lamp), L1 L2 L3: collimating lenses, ph: pinhole, P: polarizer, Q: quarter wave plate, EM: electromagnet, S: sample, A: analyzer, D: multi-channel spectrometer with a 2048-element linear silicon CCD array detector.

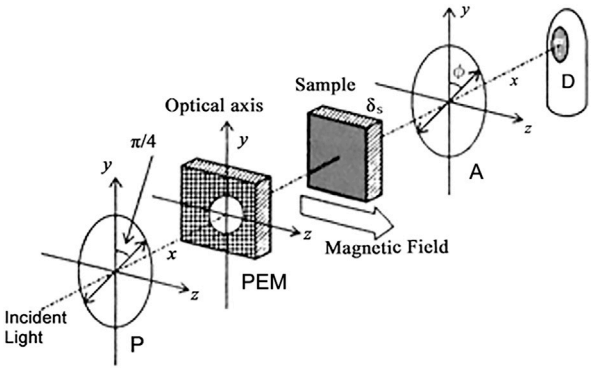

FIGURE 15 | Experimental setup for measurement of Cotton Mouton effect, which consists of a polarizer P, a photo-elastic modulator PEM, a sample, an analyzer A, and detector D.

The integral requires spectral data for ω from 0 to ∞. To get values exceeding the range of the measurement we use suitable extrapolation formulae, for which parameters are obtained so as to fit the values of visible region obtained by spectroscopic ellipsometry. Using the obtained phase shift $\Delta\theta(\omega)$ optical constants can be calculated as described in **Eq. 72**.

$$n(\omega) = \frac{1 - R(\omega)}{1 + R(\omega) + 2\sqrt{R(\omega)}\cos\Delta\theta(\omega)} \tag{72}$$
$$\kappa(\omega) = \frac{2\sqrt{R(\omega)}\sin\Delta\theta(\omega)}{1 + R(\omega) + 2\sqrt{R(\omega)}\cos\Delta\theta(\omega)}$$

From Faraday rotation θ_F and Faraday ellipticity η_F, we get the real and imaginary part of the off-diagonal element of permittivity tensor as follows.

$$\varepsilon'_{xy} = -\frac{2c}{\omega l}\left(\kappa\theta_F + n\eta_F\right)$$
$$\varepsilon''_{xy} = -\frac{2c}{\omega l}\left(n\theta_F - \kappa\eta_F\right)$$

From MOKE rotation θ_K and MOKE ellipticity η_K, we get real and imaginary part of the off-diagonal element of permittivity tensor as follows.

$$\varepsilon'_{xy} = n\left(1 - n^2 + 3\kappa^2\right) - \kappa\left(1 - 3n^2 + \kappa^2\right) \tag{73}$$
$$\varepsilon''_{xy} = \kappa\left(1 - n^2 + 3\kappa^2\right) + n\left(1 - 3n^2 + \kappa^2\right)$$

3.2.4 Measurement of Cotton-Mouton Effect

As described in subsection 2,2,5, the Cotton-Mouton effect is a MO effect in the Voigt configuration, where the applied magnetic field is perpendicular to the light propagation. The effect appears as magnetically induced optical retardation. The experimental setup (**Figure 15**) consists of a polarizer, a photo-elastic modulator PEM, a sample, an analyzer, and a detector. The polarization angle of both the polarizer and the analyzer is set 45° to the optic axis of PEM.

Assuming optical retardation is described as $\delta = \delta_0 \sin pt$, and retardation due to the sample as δ_s, the output signal of the detector is given by **Eq. 74**.

$$I_D = I_0\{1 + \cos\delta_s\cos(\delta_0\sin pt) - \sin\delta_s\sin pt\sin(\delta_0\sin pt)\} \tag{74}$$
$$\approx I_0(1 + J_2\cos\delta_s) - I_0 J_1\sin\delta_s\sin pt$$

By taking a ratio of the p-component to the DC component we obtain optical retardation of the sample.

4 CONCLUSION

First, we have described the fundamentals of the magneto-optical effect from macroscopic and microscopic stand-point, to demonstrate that off-diagonal element of electric permittivity, as well as the contribution of a diagonal element, have crucial importance for the interpretation of magneto-optical spectra of materials. Next, we described different measurement techniques of magneto-optical effect, with particular reference to the retardation modulation technique.

We hope that this review article will be useful for beginners in magneto-optics research.

AUTHOR CONTRIBUTIONS

All authors listed have made a substantial, direct, and intellectual contribution to the work and approved it for publication.

SUPPLEMENTARY MATERIAL

The Supplementary Material for this article can be found online at: https://www.frontiersin.org/articles/10.3389/fphy.2022.946515/full#supplementary-material

REFERENCES

1. K. Sato. *Light and Magnetism (revised edition)*. in Japanese: Asakurashoten Chap.3-4 (2001). p. 25–89. (ISBN 4-254-13628-5 C3342).
2. Landau LL, Lifshitz EM. Electromagnetism in continuous media. *Chap.Sec* (2003) 11, 82.
3. Argyres PN. Theory of the Faraday and Kerr effects in ferromagnetics. *Phys Rev* (1955) 97:334–45. doi:10.1103/physrev.97.334
4. Bennett HS, Stern EA. *Phys Rev* (1964) 137A:448.
5. Sato K, Ikekame H, Hongu H, Fujisawa M, Takanashi K, Fujimori H. Reflectivity Spectra in As-Polished and Annealed PtMnSb between 0.5 eV and 25 eV Measured by Synchrotron Radiation, *Proc Int Conf Ferrites* (1992). p. 1647–1650.

6. Kubo R. Statistical-mechanical theory of irreversible processes. I. General theory and simple applications to magnetic and conduction problems. *J Phys Soc Jpn* (1957) 12:570–86. doi:10.1143/jpsj.12.570
7. Kahn FJ, Persian PS, Remeika JP. Ultraviolet magneto-optical properties of single-crystal orthoferrites, garnets, and other ferric oxide compounds. *Phys Rev* (1969) 186:891–918. doi:10.1103/physrev.186.891
8. Erskine JL, Stern EA. Magneto-optic Kerr effect in Ni, Co, and Fe. *Phys Rev Lett* (1973) 30:1329–32. doi:10.1103/physrevlett.30.1329
9. Sato K. "Magneto-optical measurents" in *Magnetic measurements*" 1, eds. K. Kon H. Yasuoka, Maruzen, 2000 (in Japanese) (ISBN 4-621-04716-7 C3342)Chap.6, pp203-249.
10. Sato K. Measurement of magneto-optical Kerr effect using piezo-birefringent modulator. *Jpn J Appl Phys* (1981) 20:2403–9. doi:10.1143/jjap.20.2403
11. Sato K, Hongu H, Ikekame H, Tosaka Y, Watanabe M, Takanashi K. Magnetooptical Kerr spectrometer for 1.2-5.9 eV region and its application to FePt/Pt multilayers. *Jpn J Appl Phys* (1993) 32:989–95. doi:10.1143/jjap.32.989
12. Ishibashi T, Kuang Z, Yufune S, Kawata T, Oda M, Tani T, Magneto-optical imaging using polarization modulation method. *J Appl Phys* (2006) 100: 093903. doi:10.1063/1.2357699
13. Wang S, Nishikawa M, Ishibashi T, Sato K. Magneto-optical spectroscopy by the polarization modulation method using a multi-channel spectrometer. *Jpn J Appl Phys* (2020) 59:SEEA02. doi:10.7567/1347-4065/ab5545

Conflict of Interest: The authors declare that the research was conducted in the absence of any commercial or financial relationships that could be construed as a potential conflict of interest.

Publisher's Note: All claims expressed in this article are solely those of the authors and do not necessarily represent those of their affiliated organizations, or those of the publisher, the editors and the reviewers. Any product that may be evaluated in this article, or claim that may be made by its manufacturer, is not guaranteed or endorsed by the publisher.